

**COMPUTATIONAL HEMODYNAMIC IN CARDIOVASCULAR
SYSTEM UNDER NORMAL AND PATHOLOGICAL
CONDITIONS WITH PATIENT DATA**



Thesis submitted in partial fulfillment for the
Award of Degree
Doctor of Philosophy

By

Sumit Kumar

SCHOOL OF BIOMEDICAL ENGINEERING
INDIAN INSTITUTE OF TECHNOLOGY
(BANARAS HINDU UNIVERSITY)
VARANASI-221005
INDIA

Roll No. 17021506

Year 2023

Dedicated

To

My Loving Parents

Dr. J.P Sharma & Mrs. Sandhya Sharma

School of Biomedical Engineering
Indian Institute of Technology
(Banaras Hindu University)
Varanasi-221005



CERTIFICATE

It is certified that the work contains in this thesis titled “**Computational Hemodynamic in Cardiovascular System under Normal and Pathological Conditions with Patient Data**” by **Mr. Sumit Kumar** has been carried out under my supervision and that this work has not been submitted elsewhere for a degree.

It is further certified that the student has fulfilled all the requirements of Comprehensive Examination, Candidacy and SOTA for the award of Ph.D. Degree.

Date: 07/07/2023

Place: IIT (BHU), Varanasi

B. V. R. Kumar

S.S. Kumar Rai

Dr. Sanjay Kumar Rai
(Supervisor)
School of Biomedical Engineering
IIT (BHU), Varanasi-221005

SUPERVISOR

S.S. Kumar Rai

(Coordinator)
School of Biomedical Engineering
IIT (BHU), Varanasi-221005
समन्वयक/CO-ORDINATOR

जैव चिकित्सा अभियांत्रिकी स्कूल
SCHOOL OF BIOMEDICAL ENGG.
भारतीय प्रौद्योगिकी संस्थान (का.हि.वि.)
INDIAN INSTITUTE OF TECHNOLOGY (B.H.U.)
वाराणसी 221005/VARANASI-221005

Prof. BV Rathish Kumar
(Co-Supervisor)
Department of Mathematics
and Statistics
IIT Kanpur, 208016

School of Biomedical Engineering
Indian Institute of Technology
(Banaras Hindu University)
Varanasi-221005



DECLARATION BY THE CANDIDATE

I, **Sumit Kumar**, certify that the work embodied in this Ph.D. thesis is my own bonafide work and carried out by me under the supervision of **Dr. Sanjay Kumar Rai** from **Dec 2017 to July 2023** at the **School of Biomedical Engineering, Indian Institute of Technology (Banaras Hindu university), Varanasi**. The matter embodied in this Ph.D. thesis has not been submitted for the award of any other degree/diploma.

I declare that I have faithfully acknowledged and given credit to the research workers wherever their works have been cited in my work in this thesis. I further declare that I have not wilfully copied any other's work, paragraphs, text, data, results etc. reported in the journals, books, magazines, reports, dissertations, theses, etc., or available at websites and have not included them in this Ph.D. thesis and have not cited as my own work.

Date: 07/07/23

Place: IIT (BHU), Varanasi


Sumit Kumar

It is certified that the above statement made by the student is correct to the best of our knowledge.

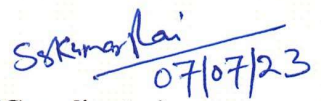
CERIFICATE BY THE SUPERVISOR AND COORDINATOR



Dr. Sanjay Kumar Rai
(Supervisor)



Prof. B.V. Rathish Kumar
(Co-supervisor)


07/07/23

(Coordinator),
SBME, IIT(BHU)

समन्वयक/CO-ORDINATOR

जैव चिकित्सा अभियांत्रिकी स्कूल
SCHOOL OF BIOMEDICAL ENGG
भारतीय प्रौद्योगिकी संस्थान (का.हि.वि.)
INDIAN INSTITUTE OF TECHNOLOGY (B.H.U.)
वाराणसी 221005/VARANASI-221005

SUPERVISOR



COPYRIGHT TRANSFER CERTIFICATE

Title of the Thesis : **“Computational Hemodynamic in Cardiovascular System under Normal and Pathological Conditions with Patient Data”**

Candidate's Name : **Mr. Sumit Kumar**

Copyright Transfer

The undersigned hereby assigns to the Indian Institute of Technology (Banaras Hindu University), Varanasi all rights under copyright that may exist in and for the above thesis submitted for the award of the Ph.D. degree.

Date: 07/07/2023

Place: IIT (BHU), Varanasi


Sumit Kumar

Note: However, the author may reproduce or authorize others to reproduce material extracted verbatim from the thesis of derivative of the thesis for author's personal use provide that the source and University's copyright notice are indicated.

Acknowledgment

I want to express my deepest gratitude to all the individuals who have supported me throughout this incredible journey of pursuing my Ph.D. and the completion of this thesis.

*First and foremost, I bow with reverence to thank “**Lord Shiva**” who enriched me with such a golden opportunity and infused the power in my mind to fulfill the task assigned to me.*

*At the outset, I would like to pay my tribute to the founder of the Banaras Hindu University, **Bharat Ratna Mahamana Pt. Madan Mohan Malviya Ji**, because of whom thousands of students put their steps towards a bright and prosperous future.*

*I would like to express my sincerest regards and love for my parents, **Dr. Jai Prakash Sharma** and **Smt. Sandhya Sharma**, for their belief in me, has been a constant source of motivation, and I am indebted to them for their sacrifices and understanding during this demanding period. Also thanks to my elder brothers **Mr. Vishal Kumar** and **Mr. Kunal Kumar** for their consistent believe , motivation and support.*

*I am immensely grateful to my supervisor, **Dr. Sanjay Kumar Rai**, and co-supervisor, **Prof. BV Rathish Kumar**, for their guidance, expertise, unwavering support, valuable and critical suggestions, boundless persuasion, scientific acumen, excellent cooperation, supervision, and kind support. Their commitment to my intellectual growth and valuable insights have been instrumental in shaping the direction of this research. I am truly fortunate to have had the opportunity to work under their supervision. I am obliged and grateful to **Dr. Prof. Om Shankar, Cardiologist and Head of the Department of Cardiology, Institute of Medical Science (BHU)**, for his valuable and critical suggestions, research collaboration, boundless persuasion, scientific acumen, excellent cooperation, supervision, and kind support. I feel very much honored, and it has been a great privilege for me to work under the mentorship of **Dr. Sanjay Kumar Rai** and **Prof. BV Rathish Kumar**.*

*I extend my sincere appreciation to the members of my Research Program Evaluation Committee (RPEC) members **Dr. Sanjeev Kumar Mahto**, Expert in the field of Tissue Engineering and Biomicrofluidics from the School of Biomedical Engineering, **Prof. Saroja Kanta Panda**, External Subject Expert, Department of Mechanical Engineering, IIT(BHU) for their expertise and engagement during committee meetings and discussions have significantly enriched the quality of this work.*

*It is my pleasure to thank all other respected faculty members of the School of Biomedical Engineering, **Prof P.K Roy** (Ex coordinator of SBME), **Prof Neeraj Sharma**, **Dr. Sanjeev Kumar Mahto**, **Dr. Pradip Paik**, **Dr. Shiru Sharma**, **Dr. A. R. Jac Fredo**, **Dr. Deepesh Kumar**, **Dr. Sudip Mukherjee**, **Dr. Gowri Balachander** and **Dr. Brijesh Kumar** for their kind cooperation and valuable suggestions during the progress of my research work.*

*I would also like to thank the **Indian Council of Medical Research (ICMR)**, **Govt. of India**, for funding and support in the research work through projects under Biomechanics Lab, SBME, IIT(BHU). Also, **Prof K.B Chandran**, Emeritus Faculty, and **Prof.M. L. (Suresh) Raghavan**, **Biomedical Engineering, University of Iowa, USA**, for research guidance and research project writing help.*

*I would like to thank Super Computing facility “**PARAM SHIVAY**” to providing a heavy computing facility in our campus for solving complex problems in less time. Also, I would like to thank Simvascular (complete pipeline from medical image data segmentation to patient specific blood flow simulation and analysis), **Prof Alison Marsden**, and her **Sandford University, USA** group members for the online repository, training, and workshop during the research work.*

*I pay my sincere thanks to **Mr. Divyanshu Singh**, **Mr. Avinash Kumar Srivastava**, **Mr. Varun Kumar Pandey**, **Dr. Anuj Srivastava**, **Mr. Bhuwaneshwari Sharan**, **Mr. Ajay Kumar**, **Mr. Bharat Kumar Vishwakarma** and all other non-teaching staff of the department who had provided me all the requirements that I needed for my research work.*

*I would like to express my special thanks and indebtedness to my most supportive seniors, **Dr. Chandan Kumar, Dr. Rati Verma, Mr. Deepak Kumar Singh, Dr. Manisha** and lab mate (**Priyanshu Soni**), and Juniors for their suggestions, help and affection.*

*No amount of thanks shall be sufficient for my friends and colleagues, **Miss. Prachi Raj Srivastava, Mr. Shreyansh, Mr. Saurabh, Mrs. Sneha Rai, Mr. Dipak Kumar** for always motivating, emotional support, love, encouragement, and moments of respite during the challenging phases of this research. Your presence and unwavering belief in me have been vital in maintaining my motivation and resilience.*

I am deeply grateful to the participants of this study who dedicated their time and efforts to providing invaluable data and insights. Their willingness to share their experiences and perspectives has greatly enriched the findings and contributions of this research.

In conclusion, the completion of this thesis would not have been possible without the collective support, guidance, and encouragement of these remarkable individuals. I am humbled by their contributions, and I am forever grateful for their presence in my life.



(Sumit Kumar)

Date: 07/07/2023

Place: IIT (BHU), Varanasi

Table of Contents

Page No.

Chapter 1

Introduction.....	01-38
1.1 Modeling and simulations of cardiovascular system.....	01
1.2 Cardiovascular system	04
1.2.1 Heart	06
1.2.2 Cardiac structure.....	07
1.2.3 Blood Vessels.....	08
1.2.4 Arteries.....	09
1.2.5 Arteries Morphology.....	10
1.2.6 Blood.....	12
1.2.7 Blood Pressure.....	13
1.3 Cardiovascular disease.....	14
1.3.1 coronary artery disease.....	15
1.3.2 Peripheral arterial disease.....	16
1.3.3 Cerebrovascular disease.....	17
1.3.4 Renal artery stenosis.....	18
1.3.5 Aortic aneurysm.....	19
1.3.6 Left heart dysfunction.....	21
1.4 Computational fluid dynamics (CFD).....	21
1.4.1 Governing Equations of blood flow.....	22
1.4.2 Finite element method (FEM).....	23
1.4.3 Finite volume method (FVM).....	26
1.5 Literature review	27
1.5.1 Recent advancement on cardiovascular disease modelling and Simulation.....	28
1.5.2 Aortic aneurysm analysis (AAA).....	29
1.5.3 coronary artery disease analysis (CAD).....	30
1.5.4 Arterial stenosis.....	32

1.5.5 Left ventricle hemodynamics.....	33
1.6 Purpose of study: Motivation.....	34
1.7 Research Objectives.....	36
1.8 Contributions of work.....	37
1.9 Thesis Structure.....	38

Chapter 2

The pulsatile 3D-Hemodynamics in a doubly afflicted human descending abdominal artery with iliac branching39-73

2.1 Introduction.....	40
2.2 Methods.....	44
2.2.1 Geometric Model	45
2.2.2 Discretization and mesh independency check.....	48
2.2.3 Computational methods	51
2.2.4 Governing equations for blood flow simulation	51
2.2.5 Simulation setup.....	52
2.3 Result and discussion	53
2.3.1 Pressure distribution in healthy and unhealthy condition.....	54
2.3.2 Velocity profile in healthy and unhealthy artery.....	57
2.3.3 Wall Shear Stress (WSS) distribution in healthy and unhealthy artery.....	59
2.3.3.1 WSS Waveform.....	59
2.3.3.2 WSS Contour Distribution	60
2.3.3.3 Local WSS contour distribution in unhealthy artery.....	60
2.3.4 Wall Shear Stress (WSS) distribution in healthy and unhealthy artery.....	64
2.3.4.1 WPs waveform.....	64
2.3.4.2 WPs contour distribution.....	65
2.3.5 Streamlines of blood flow during peak of systolic phase.....	67
2.3.6 Core vorticity and Swirling strength distribution.....	68
2.3.6.1 Vorticity distribution.....	68
2.3.6.2 Swirling strength distribution.....	69
2.3.6.3 Locally scaled axial velocity contour.....	69

2.4 Summary.....	71
------------------	----

Chapter 3

Effect of rheological models on pulsatile hemodynamics in a multiply afflicted descending human aortic network.....	74-125
--	---------------

3.1 Introduction.....	75
3.2 Methods.....	79
3.2.1 Geometric model.....	79
3.2.2 Governing equations for blood flow simulation	81
3.2.3 Non-Newtonian rheological models for blood.....	82
3.2.4 Initial and boundary conditions.....	83
3.2.5 Discretization and mesh independency check.....	83
3.2.6 Simulation setup.....	84
3.2.7 Validation.....	85
3.3 Results.....	87
3.3.1 Centerline velocity and pressure profile during the peak of systole.....	88
3.3.1.1 Centerline velocity.....	88
3.3.1.2 Centerline pressure.....	89
3.3.2 Wall shear stress effect during crucial cardiac instant.....	91
3.3.3 Wall pressure (WPs) effect during crucial cardiac instant.....	94
3.3.4 Wall shear stress contour (WSS) distribution.....	97
3.3.4.1 Cross model WSS	97
3.3.4.2 Carreau model WSS.....	98
3.3.4.3 Power model WSS.....	99
3.3.4.4 Herschel-Buckley model WSS.....	100
3.3.4.5 Newtonian model WSS.....	101
3.3.5 Sensitivity of the WSSs.....	102
3.3.6 Non-Newtonian importance factor.....	106
3.3.7 Non-Newtonian effect factor.....	109
3.3.8 Axial velocity contours.....	112
3.3.9 Streamlines of blood flow.....	115

3.3.10 Vorticity and Swirling Strength distribution.....	117
3.3.10.1 Vorticity.....	117
3.3.10.2 Swirling effect.....	117
3.4 Discussion	118
3.5 Principle Findings.....	120
3.6 Limitations and extesnsions.....	122
3.7 Summary.....	123
Chapter 4	
Influence of abdominal aortic aneurysm shape on hemodynamics in human aortofemoral arteries: A transient open-loop study.....	126-165
4.1 Introduction.....	127
4.2 Methodolgy.....	132
4.2.1 Geometry	132
4.2.2 Discretization	137
4.2.3 Governing equautions.....	138
4.2.4 Simulation setup.....	144
4.2.5 Hemodynamic parameter calculation.....	147
4.2.5.1 Time average wall shear Stress (TAWSS).....	147
4.2.5.2 Oscillatory shear index (OSI).....	147
4.2.5.3 Vortex structures.....	148
4.3 Results and discussion	148
4.3.1 Effect of aneurysms vessels dilation on velocity distributions.....	150
4.3.2 Effect of the neck angle and aneurysm's location on the velocity distribution.....	153
4.3.3 Effect of neck angle and aneurysm's location on flowlines.....	155
4.3.4 Effect of bifurcation angle on flowlines.....	157
4.3.5 Effect of neck angle on wall shear stress	159
4.3.6 Effect of aneurysm shape on hemodynamics parameters.....	161
4.3.6.1 TAWSS distribution.....	161
4.3.6.2 OSI distribution.....	162
4.3.6.3 Vortex distribution.....	163

4.4 Summary.....	164
------------------	-----

Chapter 5

Patient-Specific Blood Flow and Pressure Modelling of Suspected Coronary Artery Disease Using Open Loop System.....166-204

5.1 Introduction.....	167
5.2 Materials and Methods.....	171
5.2.1 Patient information	171
5.2.2 Image-based three-dimensional geometrical modelling.....	172
5.2.2.1 Path Planning	173
5.2.2.2 Segmentation.....	174
5.2.2.3 Lofting.....	175
5.2.2.4 Solid modelling.....	176
5.2.3 Meshing.....	177
5.2.4 Mesh Independency Test.....	180
5.2.5 Open Loop (0-3D) Finite Element Modelling.....	180
5.2.6 Governing Equations & Simulation Setup.....	182
5.2.7 Hemodynamic Parameters.....	183
5.2.8 Boundary Conditions.....	183
5.2.9 Inlet Boundary Condition.....	186
5.2.10 Coronary Boundary Conditions.....	187
5.2.11 RCR Boundary Conditions.....	191
5.3 Results	192
5.3.1 Flow rate and pressure distribution.....	192
5.3.1.1 On the outlet of the cap RCA.....	192
5.3.1.2 On the outlet of the cap LCA.....	193
5.3.2. Streamline visualization in the RCA during cardiac cycle.....	196
5.3.3 Wall shear stress (WSS) contour during cardiac cycle.....	197
5.3.4 Oscillatory Shear Index (OSI).....	198
5.3.5 Time average wall shear stress (TAWSS).....	199
5.3.6 Relative Residence Time (RRT) distribution.....	200

5.4 Discussion.....	201
5.5 Summary.....	204

Chapter 6

Image based modelling and simulation of hemodynamics in static LV human left ventricle using CT data205-233

6.1 Introduction.....	206
6.2 Methods.....	211
6.2.1 Geometry reconstruction.....	212
6.2.1.1 Image acquisition.....	212
6.2.1.2 Preparing the acquired CT Data.....	215
6.2.1.3 Manual segmentation and 3D model generation.....	217
6.2.1.4 Automatic segmentation and 3D model generation (Deep learning method).....	220
6.2.1.5 Model compatible for CFD simulations.....	223
6.2.2 Mesh Generation.....	224
6.2.3 Pulsatile boundary conditions.....	225
6.2.4 Numerical modelling.....	226
6.3 Results & discussion.....	227
6.3.1 Velocity & streamlines.....	227
6.3.2 Velocity contours of blood flow (M ₁).....	228
6.3.3 Wall pressure.....	229
6.3.4 Wall Shear stress.....	230
6.3.5 Vortex's core structures.....	231
6.4 Summary.....	232

Chapter 7

Conclusion and future work234-239

7.1 Conclusion.....	235
7.2 Future work.....	238
References.....	240
Ethical clearance.....	273
List of publications.....	274

Conferences/workshops/seminars.....	275
Research work in press news	276

List of figures

Figure no.	Figure caption	Page no.
Figure 1.1	Human cardiovascular system (“Cardiovascular system,” n.d.)	5
Figure 1.2	Schematic diagram of the four chambers of the heart and the heart valves. The arrows indicate the direction of blood flow (b) The fibrous skeleton and the four chambers of the heart. (Krishan B. Chandran, Ajit P. Yoganathan, 2010)	7
Figure 1.3	A schematic drawing depicting the left and right ventricles. The left ventricle has a more rounded shape whereas the right ventricle has a semilunar shape and wraps around the left ventricle (Krishan B. Chandran, Ajit P. Yoganathan, 2010)	8
Figure 1.4	Circulatory system (arteries, capillary, veins and arteriole) (“Capillary system CERT - Capillary - Wikipedia,” n.d.)	9
Figure 1.5	Arteries morphology (“Arteritis - Wikipedia,” n.d.)(Gasser et al., 2006)	10
Figure 1.6	Cardiac cycle (“CV Physiology Cardiac Cycle,” n.d.)	14
Figure 1.7	Common sites for the presence of atherosclerotic plaques in the human circulation (DeBaakey et al., 1985)	15
Figure 1.8	Coronary artery disease (“Blausen 0257 CoronaryArtery Plaque - Coronary artery disease - Wikipedia,” n.d.) (“Clogging of arteries treated - Parsi Teb,” n.d.)	16
Figure 1.9	Peripheral arterial disease (“Peripheral Artery Disease – Symptoms & Risks 50+ World - 50+ World,” n.d.)	17
Figure 1.10	Cerebrovascular disease and CT angiography of human brain (“CT arterial angiography,” n.d.) (Barbato et al., 2022)	18
Figure 1.11	Renal artery stenosis (“Renal artery stenosis - Symptoms and causes - Mayo Clinic,” n.d.)	19
Figure 1.12	Abdominal aortic aneurysms where, (A) shows a normal aorta. (B) shows a thoracic aortic aneurysm (which is located behind the heart), (C) shows an abdominal aortic aneurysm located below the arteries (Isselbacher, 2005)	20
Figure 2.1	Methodology designed for transient CFD simulation with step-by-step process description from Pre-processing, solver and Post Processing.	45
Figure 2.2	Reconstruction of the three-dimensional model using CT-scan DICOM image (a) segmentation of region of interest in axial view, coronal view & sagittal view (b) 3D model of artery (c) Various sectional place considered in AAA and RIAS region. Strategy adopted for local meshing (a) 3D model of artery (b)	48
Figure 2.3	Selection of local coordinates for meshing (c) Selection of spherical mesh lobe to restrict the local mesh volume (d) final mesh model	49

Figure 2.4	Mesh model of: (a) whole domain, (b) different sizes of surface element for AAA and (c) different sizes of surface element for RIIAS (d) the cross-section of the artery different with densities of the mesh in the section	50
Figure 2.5	Mesh independency test using different mesh size of mesh1, mesh 2 & and mesh 3 at different outlets	51
Figure 2.6	Pulsatile velocity inlet profile	53
Figure 2.7	(a) Central Line Pressure distribution along reference line from plane S3 at $Z = -0.17$ m in healthy abdominal artery to the end of outlet $Z = -0.36$ m during systolic phase of cardiac cycle from T_1 to T_6 using Newtonian mode (b) Central Line Pressure distribution along reference line from plane S3 at $Z = -0.17$ m in Unhealthy abdominal artery with (AAA) and (RIIAS) to the end of outlet $Z = -0.36$ m during systolic phase of cardiac cycle from T_1 to T_6 using Newtonian model.	56
Figure 2.8	(a) Velocity distribution along reference line from plane S3 at $Z = -0.17$ m in healthy abdominal artery to the end of outlet $Z = -0.36$ m during systolic phase of cardiac cycle from $T_1 = 0.1$ s to $T_6 = 0.6$ s using Newtonian model (b) Velocity distribution along reference line from plane S3 at $Z = -0.17$ m in unhealthy abdominal artery with (AAA) and (RIIAS) to the end of outlet $Z = -0.36$ m during systolic phase of cardiac cycle from $T_1 = 0.1$ s to $T_6 = 0.6$ s using Newtonian model.	58
Figure 2.9	(a) WSS distribution along medial wall contour i.e., on right side of artery from inlet to the outlet in healthy abdominal artery to the end of outlet $Z = -0.36$ m during systolic phase of cardiac cycle from $T_1 = 0.1$ s to $T_6 = 0.6$ s using Newtonian model (b) WSS distribution along medial wall contour i.e., on right side of artery from inlet to the outlet in Unhealthy abdominal artery to the end of outlet $Z = -0.36$ m during systolic phase of cardiac cycle from $T_1 = 0.1$ s to $T_6 = 0.6$ s using Newtonian model.	62
Figure 2.10	(a) and (b) WSS contour at T_1 of the healthy and unhealthy artery (c) and (d) WSS contour at T_3 of the healthy and unhealthy artery, (e) and (f) WSS contour at T_6 of a healthy and unhealthy artery using Newtonian model.	63
Figure 2.11	WSS distribution during entire cardiac cycle from T_1 to T_6 .	63
Figure 2.12	Wall pressure distribution along medial wall contour i.e., on right side of artery from inlet to the outlet in healthy abdominal artery to the end of outlet $Z = -0.36$ m during systolic phase of cardiac cycle from $T_1 = 0.1$ s to $T_6 = 0.6$ s using Newtonian model (b) Wall pressure distribution along medial wall contour i.e., on right side of artery from inlet to the outlet in Unhealthy abdominal artery to the end of outlet $Z = -0.36$ m	66

during systolic phase of cardiac cycle from $T_1 = 0.1$ s to $T_6 = 0.6$ s using Newtonian model.

Figure 2.13	Wall pressure contour during the systolic deceleration phase of cardiac cycle	67
Figure 2.14	Streamlines of the Newtonian model during peak of systole i.e., at T_3	68
Figure 2.15	Iso-surface of vorticity core region derived from of cross model during the systolic	70
Figure 2.16	Swirling strength distribution in one cardiac cycle at T_3 and $T_6 = 0.3$ and 0.6 s	70
Figure 2.17	Locally Scaled Velocity Contours on the sections S7 and S12 during the cardiac cycle	71
Figure 3.1	Apparent blood viscosity versus shear rate for different rheological models and experimental data by Merrill, Biro, and Skalak et al. (a) Carreau, Cross and HB model (b) Power-law type.	79
Figure 3.2	Reconstruction of the three-dimensional model using CT-scan DICOM image (a) segmentation of region of interest (b) 3D model of artery (c) Various sectional place considered in AAA and RIIAS region.	80
Figure 3.3	(a) Symmetricity mesh description of the AAA geometry for numerical simulation. (b) Mesh table of four mesh size Mesh1 (0.5mm), Mesh2 (1mm), Mesh3 (2mm) and Mesh3 (3 mm) (c) Mesh validation (d) Symmetric circle visualization (e) Velocity vectors on three axial plane S1, S2 and S3 (f) Velocity streamlines (g-i) Sections 1–3 (for $y^* = y/L$ 0.2, 0.5 and 0.8 respectively) at which non-dimensional axial velocity profiles are compared and velocity vectors of respective sections is plotted under steady flow conditions also comparison of numerical and experimental axial velocity profiles at the selected sections with Patel et al.	87
Figure 3.4	Velocity distribution of five rheological models along centerline line from plane S5 at $z = -0.23$ m to -0.33 m during peak of systolic phase i.e., at $T_3 = 0.3$ s.	90
Figure 3.5	Centerline pressure distribution of five rheological models from plane S5 at $z = -0.23$ m to -0.33 m during the peak of systolic phase, i.e., at $T_3 = 0.3$ s.	90
Figure 3.6	Wall shear stress distribution of five rheological models along medial plane wall i.e., on right side of artery from section S5 to the outlet of the artery to the end of outlet $Z = -0.36$ m during (a) peak of systolic phase $T_3 = 0.3$ s (b) mid of deceleration phase of systole $T_5 = 0.5$ s (c) end of systole $T_6 = 0.6$ s.	94

Figure 3.7	Wall pressure distribution of five rheological models along medial wall contour i.e., on right side of artery from section S5 to the outlet of the artery to the end of outlet $Z = -0.36$ m during (a) peak of systolic phase $T_3 = 0.3$ s (b) mid of deceleration phase of systole $T_5 = 0.5$ s (c) end of systole $T_6 = 0.6$ s.	97
Figure 3.8	WSS distribution along the aorta wall at the systole instants at T_1, T_2, T_3, T_4, T_5 and T_6 in the Cross model	98
Figure 3.9	WSS distribution along the aorta wall at the systole instants at T_1, T_2, T_3, T_4, T_5 , and T_6 in the Carreau model	99
Figure 3.10	WSS distribution along the aorta wall at the systole instants at T_1, T_2, T_3, T_4, T_5 and T_6 in the Power model	100
Figure 3.11	WSS distribution along the aorta wall at the systole instants at T_1, T_2, T_3, T_4, T_5 , and T_6 in the Herschel B model	101
Figure 3.12	WSS distribution along the aorta wall at the systole instants at T_1, T_2, T_3, T_4, T_5 and T_6 in the Newtonian model	102
Figure 3.13	Histogram of global non-Newtonian importance factor values at T_1, T_2, T_3, T_4, T_5 and T_6 .	109
Figure 3.14	WSS distribution along the descending abdominal artery wall during important time instant i.e. (T_1, T_2, T_3, T_4, T_5 AND T_6) and the non-Newtonian effect factor (NNEF) which is the relative difference between the Newtonian and non-Newtonian results is also shown.	111
Figure 3.15	(a) Velocity contours across the cross section S6, S7 and S8 of abdominal aortic aneurysms (AAA) at T_1, T_2, T_3, T_4, T_5 & T_6 in Cross (Crs) model (b) Velocity contours across the cross section S11, S12 and S13 of stenosis (RIIAS) at T_1, T_2, T_3, T_4, T_5 & T_6 in Cross (Crs) model.	114
Figure 3.16	Visualization of velocity contour at a different time step of the cardiac cycle also across various sections.	114
Figure 3.17	Streamlines of blood flow in the cross model during (a) T_3 and T_4 (b) T_5 and T_6	116
Figure 3.18	Iso-surface of vorticity core region derived from of cross model during the systolic phase of the cardiac cycle	118
Figure 3.19	Swirling strength distribution in one cardiac cycle T_1 to $T_6 = 0.1$ to 0.6 s in cross model	118
Figure 4.1	Building a model from the MRA data (a) DICOM data, image orientation, and contrast adjustment (b) generating path lines (c) segmentation and morphology operation (d) lofting the segmentation to create blood vessel (e) unioning the vessel to generate 3d single solid model.	133
Figure 4.2	Three-dimensional models of aortofemoral artery (a) Model_1 (b) Model_2 (c) Model_3 (d) Model_4 (e) Model_5	134

Figure 4.3	Dimensional details of all five models (Model_1, Model_2, Model_3, Model_4, and Model_5)	134
Figure 4.4	3D mesh view of Model_1 and with mesh independency check; (a) magnified view of mesh showing inflation layers at the inlet (b) 3D mesh Model_1 (c) magnified view of mesh in the middle of the Model_1 and right-side graph shows mesh validation using flow rate waveform at SMA outlet with respect to cardiac cycle considering fine, medium and coarse mesh sizes.	137
Figure 4.5	Mesh validation and independency check using WSS versus time at different spatial locations on the normal Model_1 artery given by the (x, y, z) coordinates in mm. WSS is shown at the selected region of interest (red colour) i.e., at the middle of the abdominal artery. The coordinates of three points taken on the superior, middle and inferior location of the wall are: P ₁ (-1.62607, 2.678528, 1.732188), P ₂ (-1.437388, 3.846733, -1.6169) and P ₃ (-1.132112, 4.305058, -5.96346).	138
Figure 4.6	The spatial domain is divided between the upstream numerical domain $\widehat{\Omega}$ (main model) and the downstream analytic domain $\widehat{\Omega} = \cup_i \widehat{\Omega}'_i$ (here the trees), separated by the coupling boundary $\Gamma_B = \cup_i \Gamma_{B_i}$ (here in green).	142
Figure 4.7	A patient-specific flow waveform measured by phase-contrast MRI (resting conditions) from an opensource vascular repository is imposed to the inlet face using a Womersley velocity profile. (a) Shows 3d Model_1 with anatomical details in which the outlet labels are as follows: CB= celiac branch, CT=celiac trunk, RRA= right renal artery, LRA=left renal artery, SM= superior mesenteric, LIIA= left internal iliac artery, RIIA=right internal iliac artery, LEIA= left external iliac artery, REIA= right external iliac artery. (b) Inflow waveforms for all five models (c) Shows a patient-specific 3-element Windkessel model with a proximal resistance (R_p), capacitance (C), and distal resistance (R_d) boundary condition is used to represent the resistance and compliance of the vasculature downstream of each outlet.	145
Figure 4.8	Computational domain and geometrical parameters used for AAA hemodynamics evaluation	150
Figure 4.9	Blood flow velocity distribution over the cross sections at the top, mid, and toe of the aneurysm and corresponding axial velocity waveform at peak systole T ₃ and peak diastole T ₅	152
Figure 4.10	Effect of neck angle on velocity distribution in the longitudinal cross-section from start of neck angle to start of iliac bifurcation in all four models at various instant of cardiac cycle (T ₀ -T ₈).	154

Figure 4.11	Neck angle and aneurysm location effect on the 3D flow pattern in the diseased case of four models (Model_1, Model_2, Model_3 & Model_4) during the cardiac cycle. The blood flow is from top to bottom, marked with a red arrow.	157
Figure 4.12	Effect of iliac bifurcation angle on streamlines of blood flow during cardiac cycle	159
Figure 4.13	Wall shear stress distribution in anterior and posterior view of all four aneurysm models of aortofemoral arteries in cardiac cycle.	161
Figure 4.14	Time average wall shear stress (TAWSS) contour in the five aortofemoral artery models	162
Figure 4.15	Oscillatory shear index (OSI) contours in the five aortofemoral artery models considering various shapes of AAA.	163
Figure 4.16	The three-dimensional vortex core region using Q-criteria and colored by the vorticity magnitude in all four diseased models of aortofemoral artery	164
Figure 5.1	Complete step by step process for cardiovascular modeling using image data, (a) image visualization, (b) Path planning (c) 2D Segmentation (i- image intensity, ii- contour of slice, iii- 2D contour ring generation & iv-lofting operation) (d) lofting operation (e) 3D volume rendering (f) Finished 3D model.	173
Figure 5.2	Path planning of CT-coronary image of patient specific model	174
Figure 5.3	2D segmentation for coronary CT- angiography data	175
Figure 5.4	Lofting operation after image segmentation	176
Figure 5.5	Computational domain and anatomical notations of 3D coronary model for hemodynamics evaluation	177
Figure 5.6	Mesh visualization of the model (a) Main 3D model (b) & (c) Inlet and outlet with boundary layer mesh view (d) Coronaries arteries mesh view	178
Figure 5.7	Delaunay criterion. According to the Delaunay criterion, no other point in the triangulation can lie beneath the circumscribing sphere (circle in 2-D) of the points that define a simplex in the triangulation. Figure (a) illustrates a Delaunay triangulation of four locations in R ² , whereas Figure (b) illustrates a non-Delaunay triangulation of the same four points.	179
Figure 5.8	Mesh independency check; depicting flowrate with respect to time step from cap_Aorta_2 of the model	180
Figure 5.9	Diagram of image-based 3D model of the patient-specific aorta and coronary arteries coupled to open-loop, inflow waveform, systemic and coronary circulations.(a) Inlet	181

	flowrate wave (b) 3D geometry of coronary model (c) Windkessel RCR boundary conditions (d) coupled to lumped parameter coronary vascular model.	
Figure 5.10	(a) Flow rate and (b) Pressure waveforms of right coronary arteries at outlets (cap_RCA, cap_RCA1, cap_RCA2, cap_RCA3, cap_RCA5, cap_RCA5) during one cardiac cycle.	194
Figure 5.11	(a) Flow rate and (b) Pressure waveforms of left coronary arteries at outlets (cap_LMCA, cap_LCA1, cap_LCA2, cap_LCA3, cap_RCA5, cap_RCA6) during one cardiac cycle.	195
Figure 5.12	Streamlines of blood flow in the (RCA) at T ₁ , T ₂ , T ₃ , T ₄ , T ₅ and T ₆ instant of cardiac cycle	196
Figure 5.13	(a) Wall shear stress contour of coronary arteries important time step of cardiac cycle i.e. during (T ₁ -T ₄), (b) during (T ₄ -T ₈).	198
Figure 5.14	Oscillatory Shear index (OSI) distribution contour map on vessel wall of (a) 3D model including LCA & RCA (b) magnified view of lateral LCA (c) magnified view of anterior lateral LCA (d) magnified view of lateral RCA (e) magnified view of anterior lateral RCA.	199
Figure 5.15	Time average wall shear stress (TAWSS) a) 3D model including LCA & RCA (b) magnified view of lateral LCA (c) magnified view of anterior lateral LCA (d) magnified view of lateral RCA (e) magnified view of anterior lateral RCA.	200
Figure 5.16	Relative Residence Time (RRT) distribution (a) Anterior view, critical region marked with dark red outline (b) Posterior view and critical region marked with dark red outline.	201
Figure 6.1	Geometrical details of the left ventricle with dynamic biological valve based on the tomographic PIV experiments (Xu and Kenjeres, 2021)	210
Figure 6.2	Workflow of image based computational modelling and simulation of blood flow in the left ventricle (LV) models	212
Figure 6.3	Hounsfield scale showing a range of Hounsfield Unit for body system	213
Figure 6.4	Schematic shows orientation of major body planes with respect to patient and their corresponding appearance on bright blood imaging sequences	214
Figure 6.5	Schematic illustrating the process of data acquisition	215
Figure 6.6	(a) Clear distinction between a preset brighter part and grey part used to set the contrasts in Mimics 18.0 (Materialise, Leuven, Belgium)	216
Figure 6.7	Image showing heart scale volume rendered data	216
Figure 6.8	CT images of heart are threshold with soft tissue (CT) scale. (a) Axial (b) Coronal (c) Sagittal View.	218
Figure 6.9	Illustration of the region grow process	219

Figure 6.10	2D CT images converted to 3D model using manual segmentation process	220
Figure 6.11	(a) Automatic segmentation workflow of the proposed approach using an ensemble of CNNs from (Kong and Shadden, 2020) (b) Network architecture of the 2D U-Net CNN model. Numbers illustrate the number of convolution kernels used.	222
Figure 6.12	Four 3D model of LV reconstructed using automatic segmentation method	223
Figure 6.13	Final ready model for CFD simulation	224
Figure 6.14	Meshing details, LV- M_1	225
Figure 6.15	Physiological Pulsatile flow condition	226
Figure 6.16	Velocity streamlines of M-1 (a) On longitudinal plane S-1 at T=0.1s and T=0.6s, Transverse plane (b) S-2, (c) S-3, (d) S-4 and (e) S-5 at T=0.1s and T=0.6s	228
Figure 6.17	Velocity contours of blood flow in model M_1 during T=0.1s & T= 0.6s	229
Figure 6.18	Wall pressure (a) M_1 early systole and (b) M_1 late diastole	230
Figure 6.19	Wall shear stress (a) M_1 early systole and M_1 late diastole	231
Figure 6.20	The three-dimensional vortex structures using Q-criteria in model (M_1) of LV at early systole and late diastole	232

List of tables

Table no.	Table caption	Page no.
Table 2.1	CT scan slice information's	47
Table 2.2	Dimensional details of geometry	47
Table 2.3	Mesh Independency Check parameter	50
Table 3.1	Effective viscosity equations of various rheological models with their parameters.	81
Table 3.2	Mesh details of geometry	84
Table 3.3	Table 3.3. Local WSS on selected point on the RIIAS surface	103
Table 3.4	Local WSS on selected point (P ₁) on the AAA surface	104
Table 3.5	Local WSS on selected point (P ₂) on the AAA surface	105
Table 3.6	Local WSS on selected point (P ₃) on the AAA surface	105-106
Table 3.7	Global importance factors for non-Newtonian models at six-time points over the cardiac	108
Table 4.1	Geometrical parameters details of Model_1	135
Table 4.2	Geometrical parameters details of Model_2	135
Table 4.3	Geometrical parameters details of Model_3	135
Table 4.4	Geometrical parameters details of Model_4	135
Table 4.5	Geometrical parameters details of Model_5	136
Table 4.6	All five models measured dimensional details	136
Table 4.7	Mesh details of all three models	138

Table 4.8	Calculated R_p , C, R_d Specification for all three models	146
Table 5.1	Basic information of the patients at the time of initial visit.	172
Table 5.2	Mesh details of coronary model	179
Table 5.3	Equation for patient-specific parametric modelling	185-186
Table 5.4	Parameter values of the coronary's outlets using coronary boundary conditions	191
Table 5.5	Calculated coronary boundary conditions parameters (R_p , C_a , R_{a-mic} , C_{min} and R_v)	192
Table 6.1	Meshing statics of Model_1	225

List of abbreviations and symbols

Abbreviation/Symbol	Details
CFD	Computational fluid dynamics
CVD	Cardiovascular disease
MRI	Magnetic resonance imaging
CT	Computed tomography
LV	Left atrium
RV	Right ventricle
RA	Right atrium
LA	Left atrium
RBC	Right blood cells
WBC	White blood cells
PAD	Peripheral Artery Disease
RAS	Renal artery stenosis
AAA	Abdominal aortic aneurysms
FEM	Finite element method
FVM	Finite Volume Method
CABG	Coronary artery bypass graft
PIV	Particle Image Velocimetry
FSI	Fluid-structure interaction
RIIAS	Right internal iliac artery stenosis
WSS	Wall shear Stress
DSA	Digital subtraction angiography
STL	Stereolithography
NNIEF	Non-Newtonian importance factor
NNEF	Non-Newtonian effect factor
DICOM	Digital Imaging and Communications in Medicine
TAWSS	Time average wall shear stress
OSI	Oscillatory shear index

PREFACE

Cardiovascular diseases (CVDs) are among the most severe public health challenges worldwide. The hemodynamic and blood-vascular interaction aspects are widely considered to have a crucial influence on the development of such illnesses. The important cardiovascular diseases linked with substantial morbidity and death include abdominal aortic aneurysm (AAA), stenosis, coronary artery disease (CAD), and irregular blood flow in the left ventricle. Knowledge of their underlying hemodynamics and biomechanics is essential to effectively diagnose, treat, and prevent these disorders. The objectives of this work is to design, develop and analyze the hemodynamics parameters in the cardiovascular disease's progression using real time patient-specific non-invasive data. Nevertheless, non-invasive blood flow monitoring technologies (such as Doppler ultrasonography and Phase Contrast MRI imaging) cannot give sufficient spatial and temporal resolution to reliably quantify some critical aspects, such as Wall Shear Stress (WSS). This type of feature is broadly known to perform a crucial role in the evolution of CVD. Without adequate hemodynamic data, it is difficult to properly assess the risk of CVDs and choose the best treatment options. Hemodynamics, heart and blood vessel illnesses are linked in various subtle ways. However, well-documented qualitative comprehension, connections, and detailed knowledge of hemodynamic circumstances are required to estimate risk and evaluate causes. Hemodynamics parameters like Wall Shear Stress (WSS), Wall Pressure (WP), Streamlines, Vorticity, Relative resilience time (RRT), Swirling Strength, Time-Average Wall Shear Stress (TAWSS) and Oscillatory Shear Index (OSI) are useful marker for blood flow dynamics studies. In this thesis work; modelling, simulation and

analysis of cardiovascular system under normal and pathological conditions with patient data have been evaluated and investigated the results using CFD method. In this work initially, investigated 3D-hemodynamics in a doubly afflicted human descending abdominal artery and compared the results with healthy condition at important cardiac instant systolic and diastolic phase then investigated the suitability and effect of rheological models in the same artery under diseased condition (AAA & RIIAS) with real time patient data from Institute of Medical Science (BHU), Varanasi, India. Furthermore; understanding the patient specific modelling and simulation of abdominal artery in multiply afflicted diseased condition from the previous work, many inferences were noted regarding the AAA shape effect and exact boundary condition implications in aortofemoral arteries. To understand the variations of AAA shape and exact boundary conditions for hemodynamics analysis, further worked on developing a methodology and investigating the morphological variation of abdominal aortic aneurysm in aortofemoral arteries using transient open-loop approach. In the systemic circulation the coronary artery provides the main blood supply to the heart and the myocardium with oxygen to allow for the contraction of the heart and thus causing circulation of the blood throughout the body. Atherosclerosis is the formation and growth of plaques within the coronary arteries. By studying plaque development and progression, researchers can gain insights into the mechanisms underlying CAD and identify potential therapeutic targets. To focus on early detection and diagnosis of CAD in the initial visit to hospital if a patient having complications in heart such as angina, weakness, nausea etc., it is important to understand the stage of CAD using computational approaches (CFD/FSI). Further in this thesis work a new methodology has been proposed for diagnosis of a suspected coronary arterial disease with patient

data using coupled (0D-3D) lumped parameter network (LPN) and CFD method. In last objective of the thesis was to develop a combination of manual and automated-based segmentation of LV and 3D modeling approaches to generate geometry from real-time CT data and to do blood flow dynamics investigation. To execute this, a 3D modeling reconstruction using image data from open source provider multi-modality whole heart segmentation (MMWHS) challenge was considered and further model was made compatible for hemodynamics studies based on pulsatile data. In summary the using computational modelling and simulation analysis of various cardiovascular diseases under various pathological condition are investigated which can help in immediate decision planning and as a diagnostic tool to the medical professional dealing with such kind of problems in CVDs.